

Orbital-lattice coupling and orbital ordering instability in iron pnictides

Dheeraj Kumar Singh^{1*}

¹*Department of Physics, Hanyang University, 17 Haengdang, Seongdong, Seoul 133-791, Korea*

Orbital-ordering instability arising due to the intrapocket nesting is investigated for the tight-binding models of pnictides in the presence of orbital-lattice coupling. The incommensurate instabilities with small momentum, which may play an important role in the nematic-ordering transition, vary from model to model besides being more favorable in comparison to the spin-density wave instability in the absence of good inter-pocket nesting. We also examine the doping dependence of such instabilities. The electron-phonon coupling parameter required to induce them are compared with the first-principle calculations.

PACS numbers: 75.30.Ds, 71.27.+a, 75.10.Lp, 71.10.Fd

I. INTRODUCTION

Iron based superconductors exhibit complex phases as a function of temperature due to the intricate interplay of spin, orbital and lattice degrees of freedom. They display a structural tetragonal-orthorhombic phase transition which either precedes the collinear spin-density wave (SDW) transition¹ or occurs simultaneously.² Moreover, the signatures of a nematic order in the orthorhombic phase have been obtained as in-plane anisotropy in several experiments such as angle resolved photoemission spectroscopy (ARPES),^{3,4} nuclear magnetic resonance (NMR) of spin fluctuations,⁵ magnetic torque measurement⁶ etc. As revealed by ARPES measurement, a significant splitting of the bands with orbital character predominantly of otherwise degenerate d_{xz} and d_{yz} orbitals in the tetragonal symmetry is observed.⁴ The origin of this ferro-type orbital order is different from that of the $(\pi, 0)$ -SDW state induced orbital ordering.^{7,9,10} Since the nematic ordering transition is marked by the simultaneous appearance of lattice distortion, orbital order as well as non vanishing spin-spin correlations with time-reversal invariance, it is therefore crucial to identify experimentally the primary factor responsible for the transition. Some progress has been made in this regard through a recent NMR experiment wherein the spin-lattice relaxation rate has been observed not to display any change at the nematic transition, thus implying a possible key role of orbital degrees of freedom.¹¹

Theoretically, the focus has been either on spin driven or orbital driven nematicity. According to the former scenario, Z_2 spin-nematic order can induce the orthorhombic lattice distortion as well as ferro-orbital order involving d_{xz} and d_{yz} orbitals although only with a small splitting between the orbitals.¹²⁻¹⁴ On the other hand, several studies have suggested a principle role for the orbital degree of freedom.¹⁵⁻¹⁹ Whereas the need to include both the spin-lattice as well as the orbital-lattice coupling has been stressed in a Monte Carlo study within a three orbital spin-fermion model.²⁰

In pnictides, Fe atom lies at the center of a tetrahedron, neighboring As atoms occupy the corners, which leads to the splitting of 5-fold degenerate d levels into

two sets. t_{2g} consists of degenerate d_{xz} , d_{yz} , and d_{xy} levels, and e_g comprises of $d_{x^2-y^2}$ and $d_{3z^2-r^2}$ levels. The degeneracy of t_{2g} levels can be partially removed by the distortion of the tetrahedron. Several tight-binding models²¹⁻²⁷ have been proposed to reproduce the Fermi surface obtained from first-principle calculations²⁸⁻³¹ and ARPES measurements³²⁻³⁴ which includes two concentric hole pockets around the Γ point and an elliptical electron pocket around the M point in the folded Brillouin zone corresponding to 2Fe/cell. The nesting between the hole and electron pockets leads to the collinear SDW state,³⁵ while doping charge carrier results into the suppression of SDW state and the appearance of superconductivity as in the case of cuprates. Magnetic and transport properties within some of these models such as minimal two-orbital model of Raghu *et al.*,²¹ three-orbital model of Daghofer *et al.*,²² and five-orbital models of Graser *et al.*²⁴ and Kuroki *et al.*²⁵ have been intensively studied. However, less attention has been paid to the orbital ordering tendency in these models especially arising due to the intrapocket nesting, which is of significant interest in the physics of pnictides particularly in the context of nematic order.

In this paper, we explore the role of orbital-lattice coupling in the orbital-ordering instability of some of the tight-binding models namely two, three, and five orbital models of Raghu *et al.*, Daghofer *et al.* and Graser *et al.*, respectively. Such instabilities may result from the intrapocket scattering enhanced by the orbital-lattice coupling. Especially, coupling to the orthorhombic distortion can remove the degeneracy of d_{xz} and d_{yz} orbitals which dominate the character of the Fermi-surface in these compounds.^{36,37}

II. HAMILTONIAN

The tight-binding part of the multi-orbital Hamiltonian to describe iron pnictide is given by

$$\mathcal{H}_0 = \sum_{\mathbf{k}} \sum_{\mu, \nu} \sum_{\sigma} T^{\mu\nu}(\mathbf{k}) d_{\mathbf{k}\mu\sigma}^{\dagger} d_{\mathbf{k}\nu\sigma}, \quad (1)$$

where $d_{\mathbf{k}\mu\sigma}^\dagger$ creates an electron in the μ -th orbital with momentum \mathbf{k} and spin σ . $T^{\mu\nu}(\mathbf{k})$ are the hopping elements from orbital μ to ν ,^{21,22,24} where μ and ν belong to the set of five d -orbitals d_{xz} , d_{yz} , d_{xy} , $d_{x^2-y^2}$, and $d_{3z^2-r^2}$ depending on the model.

The interaction part is given by

$$\begin{aligned} \mathcal{H}_{el-el} = & U \sum_{\mathbf{i},\mu} n_{\mathbf{i}\mu\uparrow} n_{\mathbf{i}\mu\downarrow} + (U' - \frac{J}{2}) \sum_{\mathbf{i},\mu<\nu} n_{\mathbf{i}\mu} n_{\mathbf{i}\nu} \\ & - 2J \sum_{\mathbf{i},\mu<\nu} \mathbf{S}_{\mathbf{i}\mu} \cdot \mathbf{S}_{\mathbf{i}\nu} + J \sum_{\mathbf{i},\mu<\nu,\sigma} d_{\mathbf{i}\mu\sigma}^\dagger d_{\mathbf{i}\mu\sigma}^\dagger d_{\mathbf{i}\nu\sigma} d_{\mathbf{i}\nu\sigma} \end{aligned} \quad (2)$$

which includes the intraorbital (interorbital) Coulomb interaction term as the first (second) term. The third term describes the Hund's coupling, and the fourth term represents the pair hopping energy. Rotation-invariant interaction is ensured provided that $U = U' + 2J$.

Finally, we consider the orbital-lattice coupling given by

$$\mathcal{H}_{e-ph} = \sum_{\mathbf{i}} g\epsilon_{\mathbf{i}} \mathcal{O}_{\mathbf{i}} + \mathcal{K}\epsilon_{\mathbf{i}}^2/2, \quad (3)$$

where the first term denotes the coupling of orbital degree of freedom to the orthorhombic strain ($\epsilon_{\mathbf{i}}$) and the second term represents the potential energy due to the strain. Here, $\mathcal{O}_{\mathbf{i}}$ is the quadrupole operator or the orbital operator ($n_{\mathbf{i}1} - n_{\mathbf{i}2}$) having B_{1g} symmetry. Subscript 1 and 2 have been used for d_{xz} and d_{yz} orbitals, respectively. Carrying out the quantization of the strain, \mathcal{H}_{e-ph} can be written as $\sum_{\mathbf{i}} g'(a_{\mathbf{i}} + a_{\mathbf{i}}^\dagger) \mathcal{O}_{\mathbf{i}} + \sum_{\mathbf{i}} \omega'(a_{\mathbf{i}}^\dagger a_{\mathbf{i}} + 1/2)$, where $a_{\mathbf{i}}^\dagger$ is the phonon creation operator, $g' = g/\sqrt{2\omega'm}$, and $\omega' = \sqrt{\mathcal{K}/m}$.

III. ORBITAL ORDERING INSTABILITIES

To investigate the orbital-ordering instability, we consider the orbital susceptibility defined as follows:

$$\chi^o(\mathbf{q}, i\Omega_n) = \int_0^\beta d\zeta e^{i\Omega_n\zeta} \langle T_\zeta [\mathcal{O}_{\mathbf{q}}(\zeta) \mathcal{O}_{-\mathbf{q}}(0)] \rangle. \quad (4)$$

Here, $\langle \dots \rangle$ denotes thermal average, T_ζ imaginary time ordering, and Ω_n are the Bosonic Matsubara frequencies. $\mathcal{O}_{\mathbf{q}}$ is obtained as the Fourier transformation of $\mathcal{O}_{\mathbf{i}}$ as defined in the previous section.

Orbital susceptibility $\chi^o(\mathbf{q})$ is calculated within the RPA-level using³⁸

$$\hat{\chi}^o(\mathbf{q}) = \hat{\chi}(\mathbf{q}) [\hat{1} + \hat{U}^o \hat{\chi}(\mathbf{q})]^{-1}, \quad (5)$$

where $\hat{1}$ is the $n^2 \times n^2$ unit matrix, where n is the number of orbitals in the model. The elements of $n^2 \times n^2$ matrix $\hat{\chi}(\mathbf{q})$ are defined by

$$\begin{aligned} \chi_{\mu\nu,\alpha\beta}(\mathbf{q}, i\Omega_n) = & -\frac{1}{N} \sum_{\mathbf{k}} \sum_{i,j} a_{j\mathbf{k}+\mathbf{q}}^{\mu*} a_{i\mathbf{k}}^\nu a_{i\mathbf{k}}^{\beta*} a_{j\mathbf{k}+\mathbf{q}}^\alpha \\ & \times \frac{n(E_i(\mathbf{k})) - n(E_j(\mathbf{k} + \mathbf{q}))}{i\Omega_n + E_i(\mathbf{k}) - E_j(\mathbf{k} + \mathbf{q})}. \end{aligned} \quad (6)$$

The interaction matrix is $\hat{U}^o = \hat{C} + 2\hat{P}$ with nonvanishing matrix elements given as $C_{n_1 n_2, n_3 n_4} = U$, $-U' + 2J$, $2U' - J$, and J for $n_1 = n_2 = n_3 = n_4$, $n_1 = n_3 \neq n_2 = n_4$, $n_1 = n_2 \neq n_3 = n_4$, and $n_1 \neq n_2 = n_3$, respectively. For the phonon-mediated interaction matrix \hat{P} ,^{17,18} $P_{11,11} = P_{22,22} = -g'^2 D(i\Omega_m)$ and $P_{11,22} = P_{22,11} = g'^2 D(i\Omega_m)$, where

$$D(i\Omega_m) = \frac{2\omega'}{\Omega_m^2 + \omega'^2}. \quad (7)$$

In the following, we set $J = U/6$ as suggested by the first-principle calculation.³⁹ A dimensionless electron-phonon coupling parameter is defined as $\tilde{\lambda} = \rho\lambda$, where ρ is the density of states at the Fermi level and $\lambda = g'^2 D(0)$. The matrix elements $\chi_{1111}(\mathbf{q})$, $\chi_{2222}(\mathbf{q})$, and $\chi_{1122}(\mathbf{q})$ are of our interest as they contribute to the orbital susceptibility corresponding to the operator \mathcal{O} defined earlier. We also note that $\chi_{1111}(q_x, q_y) = \chi_{2222}(q_y, q_x)$ due to the symmetry consideration.

A. Two-orbital model of Raghu *et al.*

Fig. 1(a) shows the Fermi surface with predominant orbital character for $\mu = 1.45$ ($n \approx 2$) in the two orbital model of Raghu *et al.* with basis consisting of d_{xz} and d_{yz} orbitals. It consists of one hole and one electron pocket at $(0, 0)$ and $(\pi, 0)$, respectively. An additional hole pocket is obtained around (π, π) instead of $(0, 0)$. An important shortcoming of this minimal model is the exclusion of d_{xy} orbital, which can contribute significantly to the Fermi surface as reported by the band-structure calculations. Despite these limitations, this model is one of the simplest models, which has been widely employed to study various properties including the $(\pi, 0)$ -SDW state in the iron pnictides.

The components of bare susceptibility corresponding to the Fermi surface (Fig. 1(a)) are shown in Fig. 1(b). Both $\chi_{1111}(\mathbf{q})$ and $\chi_{2222}(\mathbf{q})$ exhibit peaks near $(0.3\pi, 0)$ and $(0.4\pi, 0)$, respectively, in addition to that at $(\pi, 0)$. While former peak structures result from the intrapocket nesting, the latter one arises due to the interpocket nesting. Moreover in the former case, a small elongation of the electron pocket along k_x [k_y] and its predominant d_{yz} [d_{xz}] orbital character at $(\pi, 0)$ [$(0, \pi)$] results into the difference of peak positions. We also note that $\chi_{2222}(\mathbf{q})$ displays stronger peak at $(\pi, 0)$ due to the relatively good interpocket nesting between the electron pocket at $(\pi, 0)$ and hole pocket at $(0, 0)$ than between the electron pocket at $(0, \pi)$ and hole pocket at (π, π) . On the other hand, $\chi_{1122}(\mathbf{q})$ has a broad peak at $(\pi, 0)$ with the significant contribution coming from the interpocket nesting between the electron and hole pockets, and therefore it contributes significantly to the SDW instability with ordering wavevector $(\pi, 0)$ in this model. However, one bubble orbital susceptibility shows maximum near $(0, 0)$ in contrast with the spin susceptibility. This follows from the subtraction of the peak structure

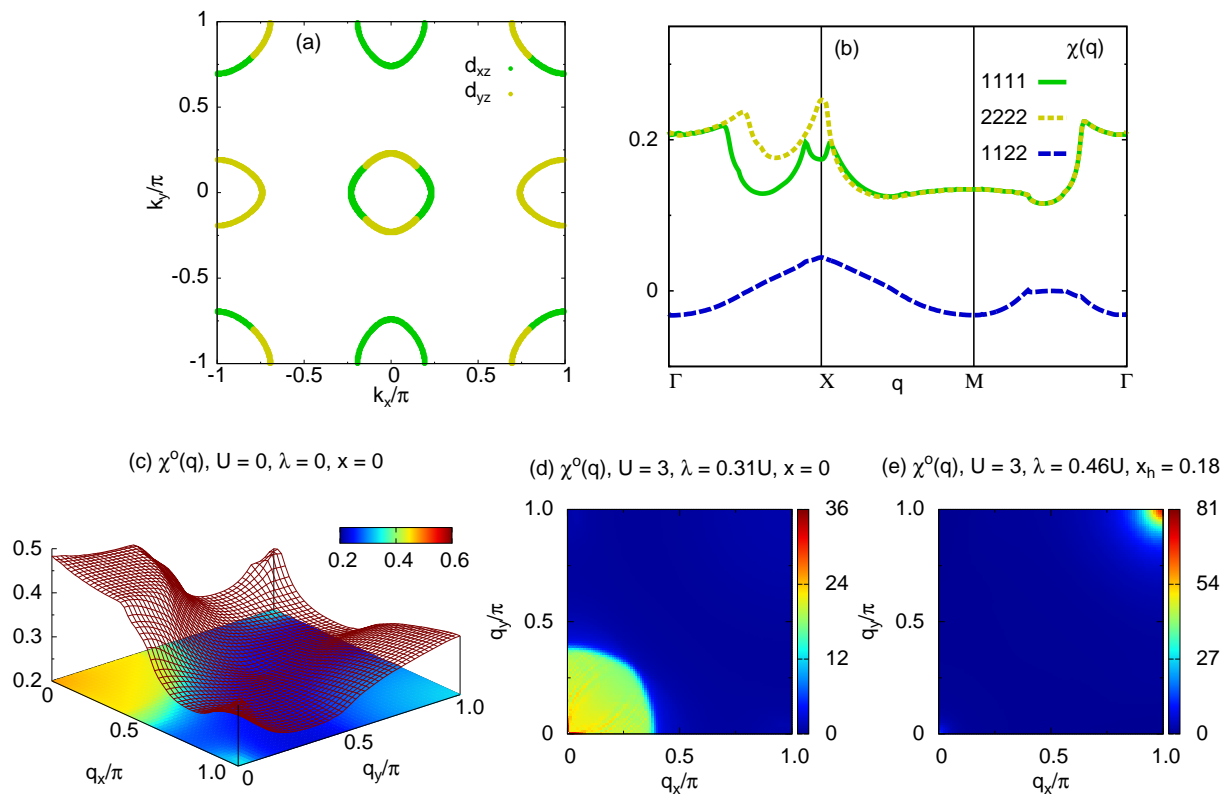


FIG. 1. (a) Fermi surface for $n \approx 2$ in the two-orbital model of Raghu *et al.* with predominant orbital distributions. (b) Components of one bubble susceptibility contributing to the orbital susceptibility. (c) Bare orbital susceptibility for undoped case. RPA-level orbital susceptibility for (d) $x_h = 0$, $\lambda = 0.31U$ and (e) $x_h = 0.18$, $\lambda_{\mathbf{q}_1} = 0.46U$, where $U = 3.0$.

of $\chi_{1122}(\mathbf{q})$ from $\chi_{1111}(\mathbf{q})$ and $\chi_{2222}(\mathbf{q})$ according to Eq. 5.

Fig. 1(d) shows the RPA orbital susceptibility diverging near $\mathbf{q} \approx (0, 0)$ for $U = 3.0$ and $\lambda = 0.3U$, which implies the existence of ferro orbital-ordering instability in this model. Here, we recall that the $(\pi, 0)$ -SDW state is stabilized in the absence of any orbital-phonon coupling as reported in earlier studies.^{10,21,35} We further note that λ as small as $\approx 0.075W$ with $U \approx 0.25W$ can lead to orbital-ordering instability, where W is estimated to be $\approx 4eV$ from the band-structure calculation so that $\lambda \approx 0.3eV$. Therefore, $\tilde{\lambda} \approx 0.12$ as the density of state at the Fermi level is $\rho \approx 0.4/eV$.

The ferro-type orbital-ordering instability remains largely unaffected for very small electron or hole doping as the Fermi surface does not display any sharp change in its shape, especially in the electron-doped regime. However, the electron pockets disappear on hole doping near $x_h \approx 0.18$ so that there is a dramatic change in the nesting condition. Consequently, an antiferro orbital-ordering instability appears due to the interpocket nesting between the hole pockets at $(0, 0)$ and at (π, π) , which is also reflected in the RPA orbital susceptibility as shown in Fig. 1(e). The critical $\tilde{\lambda} \approx 0.18$ is comparatively larger than that for the undoped case owing to the relatively poor nesting.

B. Three-orbital model of Daghofer *et al.*

The Fermi surface in the three-orbital model of Daghofer *et al.*, whose basis also includes d_{xy} orbital in addition to d_{xz} and d_{yz} orbitals, is shown (Fig. 2(a)) for the chemical potential $\mu = 0.21$ ($n \approx 4$). Several limitations of the two-orbital model such as a large hole pocket at (π, π) , the absence of an additional hole pocket at $(0, 0)$, and the contribution of d_{xy} orbital to the Fermi surface are remedied. Also, the electron pockets at $(\pi, 0)$ are elliptical in accordance with the ARPES measurement.

Fig. 2(b) shows the components of susceptibility for $n \approx 4$. Both $\chi_{1111}(\mathbf{q})$ and $\chi_{2222}(\mathbf{q})$ have peaks close to $(0.4\pi, 0)$ and $(0.6\pi, 0)$ arising due to the intrapocket nesting. The peak for $\chi_{1111}(\mathbf{q})$ results from the nesting along the minor axis of the elliptical electron pocket dominated by d_{xz} orbital at $(0, \pi)$, while the peak for $\chi_{2222}(\mathbf{q})$ follows from the nesting in the outer hole pocket dominated by d_{yz} along k_x . In addition, $\chi_{2222}(\mathbf{q})$ has a peak near $(\pi, 0)$ for the reason described in the previous section. However, $\chi_{1111}(\mathbf{q})$ does not show any peak structure close to $(\pi, 0)$ due to the absence of the hole pocket at (π, π) unlike the two-orbital model. Another difference from two-orbital model is that $\chi_{1122}(\mathbf{q})$ is negligibly small. For these reasons, the bare orbital susceptibility exhibits peak along a ring-shaped structure centered

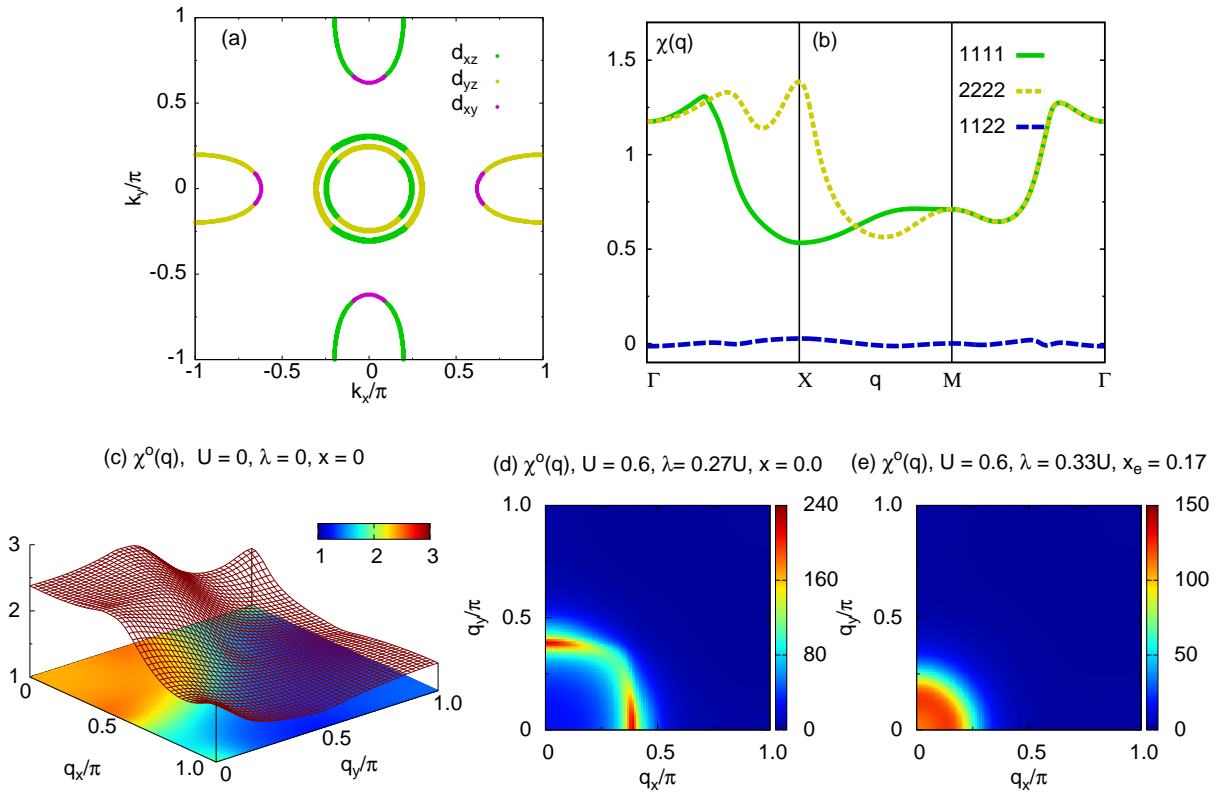


FIG. 2. (a) Fermi surface for $n \approx 4$ with the orbital character in the three-orbital model of Daghofer *et al.*. (b) Elements of one bubble susceptibility. (c) Bare orbital susceptibility for zero doping. RPA-level orbital susceptibility for (d) $x_e = 0$, $\lambda = 0.27U$ and (e) $x_e = 0.17$, $\lambda = 0.33U$, where $U = 0.6eV$.

around $\mathbf{q} = \mathbf{0}$ as shown in Fig. 2(c).

The RPA orbital susceptibility displays divergence behavior near $\mathbf{q}_1 \approx (0.4\pi, 0)$ and $(0, 0.4\pi)$ for $U = 0.6eV$ and $\lambda = 0.27U$ (Fig. 2(d)). The critical dimensionless electron-phonon coupling parameter $\tilde{\lambda} \approx 0.33$ is almost three times larger than that in the model of Raghu *et al.* because of the large density of state at the Fermi level $\rho \approx 2/eV$. Here, orbital-lattice coupling leads to an incommensurate orbital-ordering instability instead of ferro orbital-ordering instability, which results from a relatively strong intrapocket nesting along the minor axis of the elliptical electron pocket. This nesting can also play a significant role in stabilizing the magnetic order in the absence of coupling to the lattice degree of freedom. It is worthwhile to mention that this model exhibits ferromagnetic order instead of the $(\pi, 0)$ -SDW state for small intraorbital Coulomb interaction.²² Further, the hole pockets become smaller and coincident on electron doping while the electron pocket remains largely unaffected, which leads to the shifting of peak structure towards $\mathbf{q} = \mathbf{0}$ because of the intrapocket nesting of the hole pockets as shown in Fig. 2(e). While the magnitude of incommensurate nesting vector increases on hole doping.

C. Five-orbital model of Graser *et al.*

Finally, we consider the five-orbital model of Graser *et al.* The size of the electron and hole pockets are now relatively smaller in comparison to the three-orbital model as shown Fig. 3(a). The ellipticity of the electron pocket is also reduced. Another important difference being the the good nesting between the electron and hole pockets, which gives rise to $(\pi, 0)$ SDW in the undoped compound.²⁴ These features are similar to the other five-orbital models.²⁵

The components of the susceptibility are shown in Fig. 3(b). Incommensurate peak structures for $\chi_{1111}(\mathbf{q})$ and $\chi_{2222}(\mathbf{q})$ near $(0, 0)$ are weaker whereas the peak of $\chi_{2222}(\mathbf{q})$ close to $(\pi, 0)$ is strong due to the good inter-pocket nesting in comparison to the three-orbital model. The shape of the outer hole pockets is intermediate between a circle and a square, therefore there exists an intrapocket nesting along k_x , which leads to the peak in $\chi_{2222}(\mathbf{q})$ near $(0.36\pi, 0)$. Similarly, the peak structure corresponding to the small momentum in $\chi_{1111}(\mathbf{q})$ results from the intrapocket nesting of the inner hole pocket. Therefore, the bare orbital susceptibility exhibits peak near $(0, 0)$ along a ring-shaped structure as well as near $(\pi, 0)$ (Fig. 3(c)).

We note two differences in RPA-level orbital suscepti-

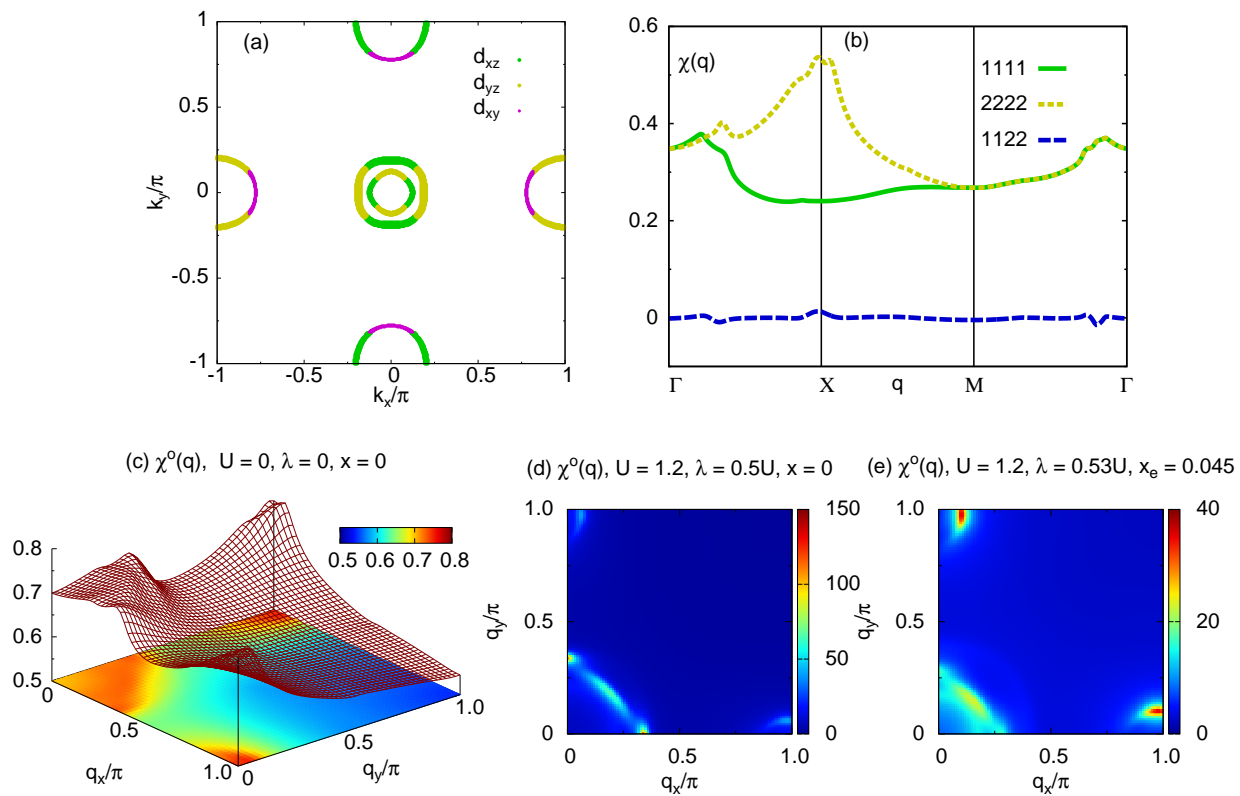


FIG. 3. (a) Fermi surface for $n \approx 6$ in the five-orbital model of Graser *et al.* with predominant orbital distributions. (b) Relevant components of one bubble susceptibility. (c) Bare orbital susceptibility in the undoped case. RPA-level orbital susceptibility for (d) $x_e = 0$, $\lambda = 0.5U$ and (e) $x_e = 0.045$, $\lambda = 0.53U$, where $U = 1.2eV$.

bility from the three-orbital model. The divergence of orbital susceptibility near $(0.36\pi, 0)$ as shown in Fig. 3(d) implies that the intrapocket nesting in the outer hole pocket is important for the orbital ordering. Secondly, the momentum corresponding to the instability dramatically gets relocated near $(\pi, 0)$ due to the improved inter-pocket nesting (Fig. 3(e)). However, the critical electron-phonon coupling parameter is $\lambda \approx 0.6$, so that $\tilde{\lambda} \approx 0.36$ as $\rho = 0.6/eV$, which is similar in magnitude to that in the case of three-orbital model.

IV. CONCLUSIONS AND DISCUSSIONS

In conclusion, we have investigated orbital-ordering instability in the models of pnictides resulting from intrapocket nesting in the presence of orbital-lattice coupling. Such instabilities are sensitive to the shape of the Fermi surface, and therefore are dependent on doping as well as on the model. In the undoped case, two-orbital model of Raghu *et al.* has an instability toward ferro orbital order whereas three-orbital model of Daghofer *et al.* displays an instability towards an incommensurate order

with small momentum. In the latter, the instability arises due to relatively strong nesting along the minor axes of the elliptical electron pocket. Such instability may also be exhibited by the model of Calderón *et al.*²⁷ because of a large major to minor axis ratio of the elliptical electron pocket. In the five-orbital model of Graser *et al.*, the instability results from the intrapocket nesting of the hole pocket. The dimensionless electron-phonon coupling parameters required to induce such instability in the models of Raghu *et al.*, Daghofer *et al.*, and Graser *et al.*, are ≈ 0.12 , 0.36 , and 0.36 , respectively. Therefore, the value of coupling parameter is smaller in the two-orbital model than that obtained from the first-principle calculation ($\tilde{\lambda} \approx 0.21$),⁴⁰ while slightly larger in the three- and five-orbital models.

ACKNOWLEDGEMENTS

The author is indebted to Tetsuya Takimoto for useful discussions. This work is supported by Basic Science Program through the National Research Foundation of Korea (NRF) funded by the Ministry of Education (NRF-2012R1A1A2008559).

- * dheeraj80@hanyang.ac.kr
- ¹ S. Nandi, M. G. Kim, A. Kreyssig, R. M. Fernandes, D. K. Pratt, A. Thaler, N. Ni, S. L. Budko, P. C. Canfield, J. Schmalian, R. J. McQueeney, and A. I. Goldman, *Phys. Rev. Lett.* **104**, 057006 (2010).
 - ² M. Rotter, M. Tegel, D. Johrendt, I. Schellenberg, W. Hermes, and R. Pöttgen, *Phys. Rev. B* **78**, 020503R (2008).
 - ³ M. Yi, D. Lu, J.-H. Chu, J. G. Analytis, A. P. Sorini, A. F. Kemper, B. Moritz, S.-K. Mo, R. G. Moore, M. Hashimoto, W.-S. Lee, Z. Hussain, T. P. Devereaux, I. R. Fisher, and Z.-X. Shen, *Proc. Natl. Acad. Sci.* **108**, 6878 (2011).
 - ⁴ T. Shimojima, T. Sonobe, W. Malaeb, K. Shinada, A. Chainani, S. Shin, T. Yoshida, S. Ideta, A. Fujimori, H. Kumigashira, K. Ono, Y. Nakashima, H. Anzai, M. Arita, A. Ino, H. Namatame, M. Taniguchi, M. Nakajima, S. Uchida, Y. Tomioka, T. Ito, K. Ki-hou, C. H. Lee, A. Iyo, H. Eisaki, K. Ohgushi, S. Kasahara, T. Terashima, H. Ikeda, T. Shibauchi, Y. Matsuda, and K. Ishizaka, *Phys. Rev. B* **89**, 045101 (2014).
 - ⁵ M. Fu, D. A. Torchetti, T. Imai, F. L. Ning, J.-Q. Yan, and A. S. Sefat, *Phys. Rev. Lett.* **109**, 247001 (2012).
 - ⁶ S. Kasahara, H. J. Shi, K. Hashimoto, S. Tonegawa, Y. Mizukami, T. Shibauchi, K. Sugimoto, T. Fukuda, T. Terashima, Andriy H. Nevidomskyy, and Y. Matsuda, *Nature* **486**, 382 (2012).
 - ⁷ M. Daghofer, Q. Luo, R. Yu, D. Yao, A. Moreo, E. Dagotto, *Phys. Rev. B* **81**, 180514(R)(2010).
 - ⁸ W. Lv, and P. Phillips, *Phys. Rev. B* **84**, 174512 (2011).
 - ⁹ K. Kubo and P. Thalmeier, *J. Phys. Soc. Jpn.* **78**, 083704 (2009).
 - ¹⁰ S. Ghosh and A. Singh, *J. Appl. Phys.* **115**, 103907 (2014).
 - ¹¹ S.-H. Baek, D. V. Efremov, J. M. Ok, J. S. Kim, Jeroen van den Brink, and B. Büchner, *Nature Mat.* **14**, 210 (2015).
 - ¹² R. M. Fernandes, A. V. Chubukov, J. Knolle, I. Eremin, and J. Schmalian, *Phys. Rev. B* **85**, 024534 (2012).
 - ¹³ K. W. Song, Y.-C. Liang, H. Lim, and Stephan Haas, *Phys. Rev. B* **88**, 054501 (2013).
 - ¹⁴ R. M. Fernandes, A. V. Chubukov, and J. Schmalian, *Nature Phys.* **10** 97 (2014).
 - ¹⁵ C.-C. Lee, W.-G. Yin, and W. Ku, *Phys. Rev. Lett.* **103**, 267001 (2009).
 - ¹⁶ C.-C. Chen, J. Maciejko, A. P. Sorini, B. Moritz, R. R. P. Singh, and T. P. Devereaux, *Phys. Rev. B* **82**, 100504(R) (2010).
 - ¹⁷ Y. Yanagi, Y. Yamakawa, N. Adachi, and Y. Ōno, *Phys. Rev. B* **82**, 064518 (2010).
 - ¹⁸ H. Kontani and S. Onari, *Phys. Rev. Lett.* **104**, 157001 (2010).
 - ¹⁹ H. Kontani and Y. Yamakawa, *Phys. Rev. Lett.* **113**, 047001 (2014).
 - ²⁰ S. Liang, A. Moreo, and E. Dagotto, *Phys. Rev. Lett.* **111**, 047004 (2013).
 - ²¹ S. Raghu, X.-L. Qi, C.-X. Liu, D. J. Scalapino, and S.-C. Zhang, *Phys. Rev. B* **77**, 220503(R) (2008).
 - ²² M. Daghofer, A. Nicholson, A. Moreo, and E. Dagotto, *Phys. Rev. B* **81**, 014511 (2008).
 - ²³ R. Yu, K. T. Trinh, A. Moreo, M. Daghofer, J. A. Riera, S. Haas, and E. Dagotto, *Phys. Rev. B* **79**, 104510 (2009).
 - ²⁴ S. Graser, T. A. Maier, P. J. Hirschfeld, and D. J. Scalapino, *New J. Phys.* **11**, 025016 (2009).
 - ²⁵ K. Kuroki, S. Onari, R. Arita, H. Usui, Y. Tanaka, H. Kontani, and Hideo Aoki, *Phys. Rev. Lett.* **101**, 087004 (2008).
 - ²⁶ H. Ikeda, R. Arita, and J. Kuneš, *Phys. Rev. B* **81**, 054502 (2010).
 - ²⁷ M. J. Calderón, B. Valenzuela, and E. Bascones, *Phys. Rev. B* **80**, 094531, (2009).
 - ²⁸ D. J. Singh, and M.-H. Du, *Phys. Rev. Lett.* **100**, 237003 (2008).
 - ²⁹ C. Cao, P. J. Hirschfeld, and H.-P. Cheng, *Phys. Rev. B* **77**, 220506(R) (2008).
 - ³⁰ G. Xu, W. Ming, Y. Yao, X. Dai, S.-C. Zhang, and Z. Fang, *EPL* **82**, 67002 (2008).
 - ³¹ K. Haule, J. H. Shim, and G. Kotliar, *Phys. Rev. Lett.* **100**, 226402 (2008).
 - ³² D. H. Lu, M. Yi, S.-K. Mo, A. S. Erickson, J. Analytis, J.-H. Chu, D. J. Singh, Z. Hussain, T. H. Geballe, I. R. Fisher, and Z.-X. Shen, *Nature* **455**, 81 (2008).
 - ³³ C. Liu, G. D. Samolyuk, Y. Lee, N. Ni, T. Kondo, A. F. Santander-Syro, S. L. Bud'ko, J. L. McChesney, E. Rotenberg, T. Valla, A. V. Fedorov, P. C. Canfield, B. N. Harmon, and A. Kaminski, *Phys. Rev. Lett.* **101**, 177005 (2008).
 - ³⁴ H. Liu, W. Zhang, L. Zhao, X. Jia, J. Meng, G. Liu, X. Dong, G. F. Chen, J. L. Luo, N. L. Wang, W. Lu, G. Wang, Y. Zhou, Y. Zhu, X. Wang, Z. Xu, C. Chen, and X. J. Zhou, *Phys. Rev. B* **78**, 184514 (2008).
 - ³⁵ P. M. R. Brydon, M. Daghofer, and C. Timm, *J. Physics: Condens. Matter* **23**, 246001 (2011).
 - ³⁶ A. M. Turner, F. Wang, and A. Vishwanath, *Phys. Rev. B* **80**, 224504 (2009).
 - ³⁷ W. Lv, J. Wu, and P. Phillips, *Phys. Rev. B* **80**, 224506 (2009).
 - ³⁸ T. Takimoto, T. Hotta, T. Maehira, K. Ueda, *J. Phys.: Condens. Matter* **14**, L369-L375 (2002).
 - ³⁹ T. Miyake, K. Nakamura, R. Arita, and M. Imada, *J. Phys. Soc. Jpn.* **79**, 044705 (2010).
 - ⁴⁰ L. Boeri, O. V. Dolgov, and A. A. Golubov, *Phys. Rev. Lett.* **101**, 026403 (2008).